

1 **Structure optimization of Spindt-type emitter**
2 **fabricated by triode high power pulsed magnetron**
3 **sputtering**

4
5 Running title: Spindt emitter optimization

6 Running Authors: Nakano et al.

7
8 Takeo Nakano ^{1,a)}, Hyuga Taniguchi ¹, Nanako Dei ¹, Makoto Ozawa ¹,
9 Md. Suruz Mian ¹, Kei Oya ¹, Katsuhisa Murakami ², and Masayoshi Nagao ²

10 ¹Faculty of Science and Technology, Seikei University, 3-3-1 Kichijoji-Kita, Musashino, Tokyo 180-
11 8633, Japan

12 ²National Institute of Advanced Industrial Science and Technology (AIST), 1-1-1 Umezono,
13 Tsukuba, Ibaraki 305-8568, Japan

14 ^{a)} Electronic mail: nakano@st.seikei.ac.jp

15
16 Spindt-type emitters were fabricated with cavities made of Al/Mo/SiO₂ using the triode
17 high power pulsed magnetron sputtering method. We explored the process parameters (gas
18 pressure and voltage of the additional cap electrode) to optimize the sharpness of the
19 emitter shape. We found that the intermediate pressure and voltage were suited to obtain
20 sharp emitters. Further, we elucidated the crucial effect of the cavity dimensions, such as
21 the cavity depth and hole diameter in the cavity ceiling, on the emitter shape. At a cavity
22 depth of 480 nm, the aspect ratio (AR) of the emitter increased monotonously with an
23 increase in the hole diameter. With a large hole diameter (900 nm) and even shallower
24 cavity (380 nm depth), we attempted to re-optimize the process parameters. Consequently,
25 a very sharp emitter cone structure with an AR exceeding 1.3 was obtained. The cap voltage
26 that produced the optimum AR was found to decrease for the larger-hole and shallower-
27 depth cavities. Finally, the applicability of the process for preparing a working emitter is
28 discussed.

1 I. INTRODUCTION

2 The Spindt-type emitter is a micro vacuum electron emitter named after C. A.
3 Spindt, who first fabricated it in 1968¹. The fabrication process included the vacuum
4 deposition of Mo onto a small cavity with a hole in its ceiling. The hole gradually closes,
5 and a Mo cone, which functions as the cathode, eventually forms inside the cavity². During
6 this process, the incident Mo atoms should ideally be concentrated along the normal
7 direction. Otherwise, more Mo atoms are deposited on the sidewall, and the hole closes
8 early, which hampers the formation of a sharp emitter structure. To achieve this
9 concentration, the evaporation source and cavity substrate must be placed far apart. Hence,
10 the deposition apparatus must be large³, resulting in low efficiency of material usage and
11 difficulties in the fabrication of large-sized cavity arrays.

12 In contrast to vacuum evaporation, the sputter deposition process is more
13 advantageous for obtaining homogeneous coatings over large areas. However, the
14 conventional sputter deposition process is not suitable for Spindt-type emitter fabrication
15 because most sputtered atoms are neutral and collide with ambient gases, causing their
16 incidence direction to be scattered and uncontrollable. In 1995, Van Veen et al. attempted
17 to apply collimated sputter deposition (CSD) for Spindt-type emitter fabrication⁴. This
18 technique, which was originally developed by Rossnagel⁵ for metallization of trench or via
19 structures for semiconductor devices⁶, involves the insertion of a physical collimator
20 between the target and substrate to limit the incidence angle of the deposited particles. CSD
21 can produce sharp tips, but it requires a high substrate temperature and subtle alignment
22 between the collimator array and the emitter array patterns; hence, it has not been widely
23 used.

1 We have been trying to apply high power pulsed magnetron sputtering (HPPMS),
2 which is a variant of ionized sputtering, for the fabrication of emitter. Ionized sputtering
3 was also pioneered by Rossnagel for trench/via metallization⁷⁻⁹, and HPPMS was
4 developed in 1999 by Kouznetsov et al.¹⁰. HPPMS, also called HiPIMS (high power
5 impulse magnetron sputtering), involves the application of pulse waveforms of very high
6 discharge power and low duty ratio to achieve increased plasma density^{11,12}. This enhances
7 the ionization of sputtered atoms so that their incidence direction can be controlled by
8 introducing a potential difference between the plasma bulk and substrate.

9 In previous studies^{13,14}, we applied the method that recently came to be known as
10 “bipolar HiPIMS”¹⁵. In this process, the target voltage is set higher than the ground
11 potential immediately after the high-power discharge to increase the potential of the
12 afterglow plasma. Using this technique, the emitter height was significantly improved
13 compared to that obtained using conventional magnetron sputtering. However, the emitter
14 was not sufficiently sharp for practical use yet. This was because of the limited usage of
15 the ionized species: the ions are subjected to the potential difference only during the
16 afterglow period of the discharge.

17 Subsequently, we developed a new approach, triode HPPMS, to increase the plasma
18 potential¹⁶. The triode HPPMS added a positively biased electrode (“cap electrode”) in
19 contact with the plasma. This ensures that the plasma potential was raised during both the
20 on and off periods of the discharge. Consequently, enhancement of the incidence direction
21 alignment of ions could be expected.

22 We applied the triode HPPMS for the preparation of the cathode of a volcano-
23 structured double-gate Spindt-type emitter¹⁷. This kind of emitter, developed by one of the

1 authors¹⁸, utilized a cavity made of plastic including photoresist (resist cavity). Following
2 the emitter formation, the cavity was completely removed using an organic solvent, leaving
3 the emitters isolated on the substrate. Subsequently, double-gate electrodes can be formed
4 for electron extraction and focusing.

5 After the process optimization, emitters with the best aspect ratio (AR; height per
6 width) of 0.7 could be prepared at an intermediate cap electrode voltage and an
7 intermediate gas pressure. Here, the alignment of ions was improved by increasing the cap
8 electrode voltage, which increased the plasma potential, or by reducing gas (Ar) pressure.
9 However, under such conditions, the compressive stress induced in the deposited Mo
10 overlayer caused the mechanically weak plastic cavity ceiling to bend, thus hastening the
11 hole closure. Therefore, the best AR value was obtained with intermediate parameters both
12 in cap voltage and in pressure.

13 In this study, we utilized a rigid cavity made of Al/Mo/SiO₂ used in the original
14 Spindt-type emitter fabrication process. This rigid cavity was used to explore the effect of
15 the deposition conditions on the Mo conical emitter without interference from cavity
16 deformation. We examined the impact of the cavity shape on emitter sharpness. Because
17 the incoming Mo particles are not completely ionized, they should have an oblique
18 component. Therefore, the effect of sidewall deposition may vary based on the cavity
19 dimensions, that is, the hole diameter and cavity depth. Finally, we examined the influence
20 of gas pressure and cap voltage on the emitter shape for shallow cavities with a large hole.
21 We found that stable emitter growth was possible under low compressive stress conditions.

1 II. EXPERIMENTAL

2 The Spindt-type Mo emitter was prepared on a microcavity substrate^{2,19}. First, the
3 SiO₂ and Mo layers were sequentially deposited on a Si substrate by chemical vapor
4 deposition and sputtering, respectively. Then the template cavity was formed by the
5 lithography of the hole pattern and dry and wet etching of Mo and SiO₂ layers (Fig. 1(a)).
6 Subsequently, Al was deposited in the oblique direction while rotating the substrate to form
7 a sacrificial layer (Fig.1 (b)). After that, emitter material was deposited from the substrate
8 normal until the hole was completely closed (Fig. 1(c)). When finishing the emitter
9 fabrication process, the Al sacrificial layer was dissolved to lift off the Mo top layer (Fig.
10 1(d)), which results were not shown in this paper.

11 In this study, the Al layer thickness was systematically varied to investigate the
12 effect of cavity dimensions on the emitter shape. As seen in the cross-sectional scanning
13 electron microscope (SEM) image of such a cavity (Fig. 2), the Al layer could be quite
14 thick to obtain the significantly narrowed hole in the cavity ceiling.

15 As the emitter material, Mo was deposited using the triode HPPMS apparatus, as
16 described in our previous report¹⁷. The anode cap of the two-inch sputter gun was insulated
17 from the electrical ground and connected to a DC power supply (current capacity of 12 A)
18 to function as an additional electrode. By applying a positive “cap voltage” V_C to this
19 electrode, the plasma potential increased¹⁶. The HPPMS discharge was generated using a
20 pulse power source (Heiwa Denki). The pulse frequency and duty ratio were set to 200 Hz
21 and 5%, respectively. The power source can be controlled only by the voltage. We adjusted
22 the voltage manually by monitoring the target current and voltage waveforms and the time-
23 averaged power calculated from them. The discharge conditions were set as follows: At the

1 start of the discharge, the time-averaged power was adjusted to 100 W with $V_C = 0$.
2 Thereafter, V_C was increased to the desired value while keeping the time-averaged target
3 current constant.

4 The target was a Mo disk with a diameter and thickness of 50 and 3 mm,
5 respectively. According to the magnetron configuration, an erosion track was formed on
6 the target as a ring, with the deepest part being 23 mm in diameter. The target-to-substrate
7 (T-S) distance was 74 mm. In this experiment, the substrate was not intentionally heated
8 or cooled. The deposition system was evacuated to $<5 \times 10^{-5}$ Pa before deposition, and
9 Ar gas of 5N purity was supplied. When the Ar gas flow rate was set to 10 sccm, the gas
10 pressure was 0.6 Pa. Higher or lower pressures were obtained by throttling the evacuation
11 valve or reducing the gas flow rate, respectively.

12 Prior to the actual deposition experiments, a stage equipped with three quartz
13 crystal microbalance (QCM) thickness monitors was placed inside the HPPMS apparatus
14 to measure the deposition rate. The stage was approximately the same size as the substrate
15 holder used in the deposition experiment. The details of the QCM stage are provided in our
16 previous report²⁰. In this study, a monitor placed at the center of the stage was used. This
17 monitor was located near the position where the substrates were placed in the deposition
18 experiments. The monitor was connected to a QCM controller (Inficon, SQM-160), and
19 the variation in the deposition rate under different process conditions was recorded.

20 The emitter deposition batches were run as follows. With the discharge conditions
21 set, the target was pre-sputtered for 10 min, and then the shutter was opened. The typical
22 deposition time required to completely close the hole in the ceiling of the cavity was 30–
23 90 min. In each deposition batch, a bare Si (100) substrate was placed next to the cavity

1 substrate. It was treated with diluted HF, rinsed with distilled water, and then set to the
2 substrate holder.

3 Following Mo deposition, the cavity substrate was cleaved at the center, and the
4 plan view and cross-sectional images were obtained using a secondary electron microscope
5 (SEM, JEOL, JSM-6510). We defined the AR of the emitter as the ratio of the half-height
6 of the emitter divided by the full-width at half height. We adopted this definition because
7 the hem of the emitter was curved; thus, the width at the emitter bottom was difficult to
8 determine. The AR was determined for 4–10 emitters, and their average and standard error
9 were calculated.

10 A bare Si substrate sample was also observed using cross-sectional SEM to evaluate
11 the film structure and thickness. In addition, X-ray diffraction (XRD) of the sample was
12 measured by a diffractometer (Rigaku, Ultima-IV) to elucidate the Mo film orientation and
13 stress condition. The X-ray source was Cu K α , and the conventional $\theta - 2\theta$ mode was
14 used. In the XRD pattern of the samples within $2\theta = 10^\circ - 80^\circ$, only the Mo (110) peak
15 could be observed. Using the lattice plane spacing of Mo (110), the biaxial stress σ was
16 evaluated using the following relation²¹

$$17 \quad \sigma = -\frac{E}{2\nu} \frac{d - d_0}{d_0}, \quad (1)$$

18 where d is the measured lattice spacing of the film and $d_0 = 2.225 \text{ \AA}$ is the lattice
19 spacing of Mo (110) in the powder diffraction data (PDF 00-004-0809). $E = 323 \text{ GPa}$
20 and $\nu = 0.31$ are the Young's modulus and Poisson's ratio of Mo, respectively²².

1 III. RESULTS AND DISCUSSION

2 A. *Effects of cap voltage and gas pressure*

3 Figure 3 demonstrates the deposition rate measured by the QCM monitor at Ar gas
4 pressures of 0.3 and 0.6 Pa. On increasing the cap voltage from $V_C = 0$, the deposition rate
5 increased slightly, showed a maximum at $V_C \approx 20$ V, and then decreased to a constant
6 value less than that at $V_C = 0$. At other gas pressures (0.16 and 1.0 Pa), a similar tendency
7 was observed. This behavior should be due to the potential and density distribution of the
8 plasma, both of which are affected by the positive cap voltage. However, we do not have a
9 clear explanation for it. The film thickness obtained from the cross-sectional SEM image
10 is consistent with these results.

11 We conducted the emitter fabrication experiments using a cavity with a hole
12 diameter of 540 nm and depth of 280 nm, similar to the resist cavity used in the previous
13 study¹⁷. The SEM images presented in Fig. 4 indicate the influence of the cap voltage V_C
14 on the emitter shape prepared at an Ar gas pressure of 0.3 Pa. The best AR value was
15 1.06 ± 0.08 ($n = 4$) obtained at $V_C = 40$ V (Fig. 4(b)).

16 The trend of the maximum AR occurring at an intermediate cap voltage was similar
17 to that reported in the previous study using the resist cavity. This could be explained by the
18 counteracting effects of the directionality of the incident ions and the compressive stress in
19 the Mo overlayer. The increase in the plasma potential leads to an increase in the normal
20 component of the incident ion velocity, which improves the alignment of ions. However,
21 the higher plasma potential increases the incident energy of ions, thereby increasing the
22 compressive stress in the film²³. The compressive stress causes the bending of the cavity

1 ceiling and the inward collapse of the Mo overlayer around the hole. Both of these hasten
2 the closure of the hole and thus obstruct the formation of a sharp emitter.

3 Figure 5 illustrates the influence of the cap voltage and Ar gas pressure on the AR.
4 As shown in Fig. 5(a), the AR reaches a maximum at the intermediate cap voltage. The
5 pressure dependence of AR at $V_C = 40$ V, as shown in Fig. 5(b), shows that too high or
6 low a gas pressure also degrades the AR value. A higher gas pressure leads to the more
7 scattering of accelerating ions within the sheath, which leads to misalignment of ions.
8 Conversely, a lower gas pressure may improve the alignment but increase the compressive
9 stress in the film owing to the more energetic incidence. Thus, the competition between the
10 incidence direction alignment and compressive stress increase occurs based also on this
11 parameter.

12 The best AR value increased when the Al/Mo/SiO₂ cavity was used instead of the
13 resist cavity (for which the best AR was 0.7). This could be attributed to the suppression
14 of cavity bending on using the rigid cavity. Notably, the gas pressure at which the AR was
15 highest for the Al/Mo/SiO₂ cavity was lower than that for the resist cavity. This suggests
16 that the competition described above shifted towards more directivity and higher
17 compressive stress conditions. However, the film collapses, and the degradation of the AR
18 value occurs for a considerably high cap voltage. This is confirmed by the steeper collapse
19 angle of the Mo overlayer around the hole at $V_C = 60$ V (Fig. 4(c)) in comparison to that
20 at lower cap voltages ((Figs. 4(a) and 4(b)).

21 The Mo cone, observed in Fig. 4(b), is suitable for emitter operation. However,
22 when we proceeded with the emitter fabrication process, delamination of the Mo overlayer
23 occurred owing to compressive stress. Accordingly, we estimated the stress using XRD.

1 Figure 6 presents the results of XRD measurement of Mo films deposited on the bare Si
2 (100) substrate at 0.3 Pa for 30 min at various anode cap voltages. Figure 6(a) shows the
3 wide patterns for $2\theta = 20^\circ - 80^\circ$. The Mo films were found to be highly oriented toward
4 (110), which is the densest plane of the body-centered cubic crystal to which the Mo metal
5 belongs. The (110)-oriented film growth of Mo has been frequently observed in various
6 deposition methods, including conventional DC sputter deposition²⁴ and pulsed laser
7 deposition²⁵. Figure 6(b) shows narrow patterns around the Mo (110) peak. The vertical
8 axis of this graph was plotted on a logarithmic scale. All the peak positions were shifted to
9 smaller angles compared to the one corresponding to the (110) spacing of the Mo powder
10 sample (40.55°), which indicates the existence of biaxial compressive stress in the film²¹.
11 The shift was most prominent at $V_C = 40$ V and was diminished at both smaller and larger
12 cap voltage values.

13 Using Eq. 1, the compressive stress in the films was calculated and plotted as
14 functions of (a) V_C (at 0.3 Pa) and (b) Ar pressure (at $V_C = 40$ V), as shown in Fig. 7. The
15 film stress increased with the decrease in the gas pressure (Fig. 7(b)), whereas it reached a
16 maximum at $V_C = 40$ V (Fig. 7(a)). This shows that too high a cap voltage and plasma
17 potential lead to the relaxation of the compressive stress. Windischmann summarized the
18 dependence of compressive stress on incident particle momentum in his review²⁶; as the
19 momentum increases, the film stress changes abruptly from tensile to compressive at a
20 certain point. After the compressive stress value reaches a maximum, it relaxes in the larger
21 momentum region. He ascribed this behavior to the plastic flow of the films caused by
22 excessively high compressive stress. The results obtained from our experiment agreed with
23 this tendency. With the increase in the cap voltage and subsequent increase in the particle

1 energy and momentum, the compressive stress value initially increased, then reached a
2 maximum, and finally relaxed.

3 Interestingly, the Mo (110) peak became much higher at $V_c = 60$ V, where plastic
4 flow was assumed to occur. This agrees with the discussion in a paper by Window²⁷, in
5 which the Mo film structures were studied using unbalanced magnetron sputtering with
6 substrate biasing. With increasing substrate bias, Window found that the compressive stress
7 reached a maximum value, and the Mo (110) peak was enhanced. He attributed these
8 phenomena to the fact that the wire drawing of Mo favors the (110) direction. During the
9 wire drawing process, Mo was under biaxial stress condition, similar to the film growth
10 process.

11 **B. Effect of hole size on the emitter shape**

12 In the course of experimental trials conducted to overcome the Mo overlayer
13 delamination as described earlier, we found that the AR of the emitter cone was also
14 strongly influenced by the cavity dimensions. Specifically, if a deeper cavity (i.e., a cavity
15 with a thicker SiO₂ layer) or a smaller hole was used, the AR of the fabricated emitter
16 decreased. To evaluate this effect systematically, we prepared a cavity with a shallow depth
17 (thin SiO₂ layer) and a large hole through the Mo layer. Then, the Al sacrificial layer was
18 obliquely deposited at various thicknesses. By increasing the Al deposition thickness, the
19 hole diameter was reduced by the sidewall deposition of Al. It was confirmed by observing
20 the cross-sectional SEM images of the cavities. Finally, Mo was deposited on these cavities
21 to form emitters.

22 Figure 8 shows the cross-sectional SEM images of emitters deposited onto cavities
23 with different hole diameters. The thickness of the SiO₂ layer was 480 nm. The deposition

1 conditions were an Ar gas pressure of 0.3 Pa and a cap voltage of 40 V, which led to the
2 optimum AR value in the experiment described in Section A. Clearly, the larger the hole
3 diameter, the larger the AR value. The deposition time was 30 min for the cavities shown
4 in Fig. 8(a)–(c), while for the cavity with the largest hole diameter (795 nm) (Fig. 8(d)),
5 the hole could not be closed within 30 min; thus, the time was extended to 45 min.

6 The influence of hole size on the AR is shown in Fig. 9. The AR increased
7 monotonously with an increase in the hole diameter. **It should be noted that the result also**
8 **implied that the cavity depth affected the AR value.** For the cavity with a SiO₂ layer
9 thickness of 280 nm and a hole diameter of 580 nm, which appeared in Section A, the AR
10 value was 1.06 under the same deposition conditions. **On the other hand, the AR was only**
11 **0.64 at a similar hole diameter of 600 nm when the SiO₂ thickness was 540 nm (Fig. 8(c)).**
12 This suggests that the AR also depends on the cavity depth; it becomes larger for shallower
13 cavities.

14 The results shown in Figs. 8 and 9 imply that a considerable fraction of Mo
15 particles was incident on the substrate at a tilt with respect to the normal in our experiments.
16 Such particles were deposited on the sidewall of the cavity hole, which accelerated its
17 closure. While Mo ions certainly played an important role in the process, which was
18 confirmed by the influence of the cap voltage on the AR (Figs. 4 and 5), Mo neutral atoms
19 also remained and were incident on the substrate, reflecting the effects of target–substrate
20 geometry and scattering by the ambient Ar gas atoms during the transport²⁸.

21 In our experimental setup, for the erosion track diameter of 23 mm and T-S distance
22 of 74 mm, the calculated line-of-sight angle from the substrate normal was 9.5°. This angle,
23 intriguingly, is close to the angle between the hem of the emitter cone and the edge of the

1 hole in the cavity ceiling, as indicated by the solid yellow lines in Fig. 8. Horkel et al.
2 reported that the angular distribution of incident atoms (including heavy metals such as W
3 or Cu) was strongly affected by the Ar gas pressure even at a low range of 0.3–0.5 Pa for
4 the T-S distance of 95 mm²⁹. They found that the angular distribution was considerably
5 broadened with an increase in the gas pressure in this pressure range. Therefore, in our
6 experiment, we assumed that a considerable amount of Mo neutral atoms impinged at
7 slanted angles.

8 The effect of the cavity dimension in such a case can be discussed in relation to the
9 via-filling simulation by Smy et al.³⁰. Considering angular distribution, they reported that
10 the wider the via diameter and the shallower its depth, the better the bottom coverage. This
11 can be ascribed to the difference in the solid angle from the bottom of the via to the particle
12 incidence direction. **In this study, similarly, the narrower hole and the deeper cavity reduce**
13 **the solid angle from the cavity bottom to the hole. In other words, the number of incident**
14 **Mo atoms decreases at the bottom of the cavity due to the geometrical restriction by the**
15 **hole edge. Hence, the effective deposition rate of Mo decreases here.** Therefore, the emitter
16 cannot grow sufficiently vertically before hole closure, resulting in degraded sharpness of
17 the emitter. Furthermore, the Al sacrificial layer thickness was increased for cavities with
18 smaller hole diameters because the hole was narrowed by the oblique deposition of Al.
19 This may also cause the degradation of emitter sharpness.

20 **C. Influence of cap voltage for cavity with large hole**

21 During the experiment, concerning the effect of cavity dimension presented in
22 Section B, we noticed that the inward collapse of the Mo overlayer around the hole was
23 more prominent for the larger hole (e.g., Fig. 8(d)) in comparison with that for the smaller

1 hole (Fig. 4(b)). This can be attributed to the larger overlayer thickness required to close
2 the hole of a large diameter. In this case, the accumulated compressive stress pushed the
3 film inward at its periphery, thereby accelerating hole closure and hampering the sharp
4 emitter formation. Therefore, the optimum cap voltage may shift to a lower value to reduce
5 the film stress at the expense of the directivity of the incident ions.

6 Accordingly, we re-evaluated the influence of the cap voltage dependence on the
7 AR of the emitter for a shallow cavity with a large hole. In this series of emitter fabrication,
8 we prepared a shallower cavity with a SiO₂ layer thickness of 300 nm (note that the SiO₂
9 layer thickness was 480 nm for the cavities shown in Fig. 8). Figure 10 presents the results
10 for the cap voltage dependence of the AR. In these cases, 60–75 min of deposition time
11 was required to close the hole owing to the large hole diameter. **The AR showed a**
12 **maximum around a cap voltage of 10–15 V. It was clearly lower than that (40 V) for the**
13 **smaller hole case shown in Fig. 4.** In addition, the maximum AR value of 1.32, which was
14 obtained at 0.3 Pa and $V_c = 10$ V, was significantly larger than that obtained for the deeper
15 cavity, shown in Fig. 8(d).

16 Figure 11 shows the emitter that yielded the maximum AR. The emitter had an
17 excellent sharp shape suitable for the effective emission of electrons and was comparable
18 to those fabricated by conventional evaporation techniques. For example, Itoh et al.
19 obtained a Mo emitter with an AR of 1.3 by electron beam (EB) evaporation³¹. However,
20 during the fabrication of emitters by EB evaporation, an elevated substrate temperature as
21 high as 200–500 °C is necessary to reduce the tensile film stress and obtain a sharp tip
22 apex³². In contrast, the triode HPPMS resulted in a similar AR without substrate heating.
23 This is one of the advantages of the proposed method.

1 For the electrical emission, the radius of curvature (RoC) of the tip apex is a crucial
2 parameter. Due to the limited resolution of our SEM used in this study, we could not
3 systematically determine the RoC of emitters. However, the positive correlation between
4 AR and RoC is evident, as shown in Figs. 4, 8. Among emitters shown in Fig. 4, the apex
5 was the sharpest when AR was the largest (Fig 4(b)). In Fig. 8, the keener apex of higher
6 AR emitters was also apparent. It should also be noted that several theoretical
7 considerations^{33,34} involve AR as a parameter and show that the larger AR positively affects
8 the emission performance. In addition, in emitters fabricated by conventional vacuum
9 deposition, their apex is not always ideally sharp³².

10 Unfortunately, the emitter shown in Fig. 11 does not function at this stage after the
11 lift-off process of the sacrificial Al layer and the Mo layer above it. This is because the gate
12 electrode (i.e., the Mo layer between the SiO₂ and Al layers) is far below the emitter tip;
13 thus, the extraction field cannot be applied effectively. Nevertheless, the findings of this
14 study will be of substantial help in the fabrication of Spindt-type emitters by HPPMS.

15 First, it was found that, by controlling the cavity structure, sharp emitters could be
16 successfully fabricated at a cap voltage as low as 10 V, at which the strong compressive
17 stress in the Mo overlayer could be avoided. Using a cavity with an appropriate ratio of
18 hole diameter to depth, which can be controlled independently by the photolithography
19 pattern and the SiO₂ thickness, we can fabricate suitable height emitters aligned with the
20 gate electrode.

21 Second, the availability of emitters under less compressive stress conditions may
22 allow us to rethink the use of the resist cavity. That is, by preparing shallow cavities with
23 a large hole using resist layers, it may be possible to fabricate isolated emitter tips on the

1 substrate. As another approach for preparing a freestanding emitter tip array, **we may be**
2 **able to dissolve the SiO₂ layer of the cavity (See Fig. 1) with structures above it.** After that,
3 we can fabricate the volcano-structured double-gate emitters as described in our previous
4 publication¹⁸.

5 Finally, the ionization rate of the sputtered atoms was reaffirmed as an essential
6 factor for the sharpness of the emitter. In this study, we suggested the presence of neutral
7 atoms, which were incident on the cavity obliquely and accelerated the hole closure even
8 at Ar gas pressures of 0.3–0.6 Pa. If the ionization rate increases, they can be aligned by
9 the potential difference between the plasma and substrate, resulting in the formation of
10 sharper emitters. It can be achieved by optimizing the discharge parameters of HPPMS or
11 exploring alternative emitter materials to Mo. We plan to take up further research in this
12 direction.

1 IV. SUMMARY

2 In this study, we considered the fabrication of a Spindt-type emitter by triode
3 HPPMS using a rigid cavity made of SiO₂, Al, and Mo layers and investigated the effects
4 of the Ar pressure and cap electrode voltage on the AR of the emitter. The maximum value
5 of AR was obtained at the intermediate value of each, which was ascribed to the
6 competition between the directivity of the incident particles and compressive stress in the
7 overlayer. By varying the diameter of the hole in the cavity ceiling, the AR of the emitter
8 was found to be larger for cavities with larger holes, suggesting the presence of a
9 considerable fraction of oblique incident particles, probably originating from neutral
10 sputtered atoms. For shallow cavities with a large hole diameter, the emitter with the
11 highest AR (1.32) was obtained under low compressive stress conditions. This opens the
12 possibility of fabricating emitters with excellent characteristics by tuning the cavity
13 structure.

14

1 **ACKNOWLEDGMENTS**

2 This work was partly supported by JSPS KAKENHI (Grant Number 17K05106). The
3 authors acknowledge the support of Prof. Shigeo Satokawa and Prof. Kazumasa Ohshima
4 for their help with the XRD measurements. A part of this work was conducted at the AIST
5 Nano-Processing Facility, supported by “Nanotechnology Platform Program” of the
6 Ministry of Education, Culture, Sports, Science and Technology (MEXT), Japan.

7

8 **AUTHOR DECLARATIONS**

9 **Conflict of Interest**

10 The authors have no conflicts of interest to disclose.

11

12 **DATA AVAILABILITY**

13 The data that support the findings of this study are available from the corresponding author
14 upon reasonable request.

15

1 **References**

- 2 ¹ C. A. Spindt, J. Appl. Phys. **39**, 3504 (1968).
- 3 ² M. Nagao and T. Yoshida, Microelectron. Eng. **132**, 14 (2015).
- 4 ³ A. A. Talin, K. A. Dean, and J. E. Jaskie, Solid. State. Electron. **45**, 963 (2001).
- 5 ⁴ G. N. A. van Veen, B. Theunissen, K. van de Heuvel, R. Horne, and A. L. J. Burgmans,
6 J. Vac. Sci. Technol. B **13**, 478 (1995).
- 7 ⁵ S. M. Rossnagel, D. Mikalsen, H. Kinoshita, and J. J. Cuomo, J. Vac. Sci. Technol. A
8 **9**, 261 (1991).
- 9 ⁶ C. Cabral, C. Lavoie, C. Murray, A. Pyzyna, and K. Rodbell, J. Vac. Sci. Technol. A
10 **38**, 040803 (2020).
- 11 ⁷ S. M. Rossnagel and J. Hopwood, Appl. Phys. Lett. **63**, 3285 (1993).
- 12 ⁸ U. Helmersson, M. Lattemann, J. Bohlmark, A. P. Ehiasarian, and J. T. Gudmundsson,
13 Thin Solid Films **513**, 1 (2006).
- 14 ⁹ J. A. Hopwood, *Ionized Physical Vapor Deposition* (Academic Press, San Diego, 1999).
- 15 ¹⁰ V. Kouznetsov, K. Macák, J. M. Schneider, U. Helmersson, and I. Petrov, Surf. Coat.
16 Technol. **122**, 290 (1999).
- 17 ¹¹ K. Sarakinos, J. Alami, and S. Konstantinidis, Surf. Coat. Technol. **204**, 1661 (2010).
- 18 ¹² J. T. Gudmundsson, N. Brenning, D. Lundin, and U. Helmersson, J. Vac. Sci. Technol.
19 A **30**, 030801 (2012).
- 20 ¹³ T. Yoshida, M. Nagao, T. Nishi, N. Koda, and T. Nakano, in *Proc. IDW/AD '12, 19th*
21 *Int. Disp. Work.* (2012), pp. 1791–1794.
- 22 ¹⁴ T. Yoshida, M. Nagao, N. Koda, T. Nishi, H. Ohsaki, and T. Nakano, in *25th Int. Vac.*
23 *Nanoelectron. Conf.* (IEEE, 2012), pp. 1–2.
- 24 ¹⁵ J. Keraudy, R. P. B. Viloan, M. A. Raadu, N. Brenning, D. Lundin, and U. Helmersson,
25 Surf. Coat. Technol. **359**, 433 (2019).
- 26 ¹⁶ T. Nakano, T. Umahashi, and S. Baba, Jpn. J. Appl. Phys. **53**, 028001 (2014).

- 1 ¹⁷ T. Nakano, T. Narita, K. Oya, M. Nagao, and H. Ohsaki, *J. Vac. Sci. Technol. B* **35**,
2 022204 (2017).
- 3 ¹⁸ M. Nagao and S. Yoshizawa, in *2014 27th Int. Vac. Nanoelectron. Conf.* (IEEE, 2014),
4 pp. 226–227.
- 5 ¹⁹ C. A. Spindt, I. Brodie, L. Humphrey, and E.R. Westerberg, *J. Appl. Phys.* **47**, 5248
6 (1976).
- 7 ²⁰ T. Nakano and S. Baba, *Vacuum* **80**, 647 (2006).
- 8 ²¹ M. Ohring, *Materials Science of Thin Films*, 2nd ed. (Academic Press, San Diego, CA,
9 2002).
- 10 ²² D. R. Lide and E. Al., editors , *CRC Handbook of Chemistry and Physics*, 60th ed.
11 (CRC, Cleavland, Ohio, 1979).
- 12 ²³ H. Windischmann, *Crit. Rev. Solid State Mater. Sci.* **17**, 547 (1992).
- 13 ²⁴ F. Martin, P. Muralt, and M.-A. Dubois, *J. Vac. Sci. Technol. A* **24**, 946 (2006).
- 14 ²⁵ O. Fruchart, S. Jaren, and J. Rothman, *Appl. Surf. Sci.* **135**, 218 (1998).
- 15 ²⁶ H. Windischmann, *J. Vac. Sci. Technol. A* **9**, 2431 (1991).
- 16 ²⁷ B. Window, *J. Vac. Sci. Technol. A* **7**, 3036 (1989).
- 17 ²⁸ S. Mahieu, K. Van Aeken, and D. Depla, in *Reactive Sputter Deposition*, edited by D.
18 Depla and S. Mahieu (Springer, Berlin, Heidelberg, 2008), pp. 199–227.
- 19 ²⁹ M. Horkel, K. Van Aeken, C. Eisenmenger-Sittner, D. Depla, S. Mahieu, and W. P.
20 Leroy, *J. Phys. D: Appl. Phys.* **43**, 075302 (2010).
- 21 ³⁰ T. Smy, K. L. Westra, and M. J. Brett, *IEEE Trans. Electron Devices* **37**, 591 (1990).
- 22 ³¹ S. Itoh, T. Watanabe, K. Ohtsu, M. Taniguchi, S. Uzawa, and N. Nishimura, *J. Vac.*
23 *Sci. Technol. B* **13**, 487 (1995).
- 24 ³² C. A. Spindt, I. Brodie, C. E. Holland, and P. R. Schwoebel, in *Vacuum*
25 *Microelectronics*, edited by W. Zhu (Wiley, New York, 2001), Chap 4.
- 26 ³³ D. Nicolaescu, M. Nagao, V. Filip, S. Kanemaru, and J. Itoh, *J. Vac. Sci. Technol. B*
27 **21** 1550 (2003).



This is the author's peer reviewed, accepted manuscript. However, the online version of record will be different from this version once it has been copyedited and typeset.
PLEASE CITE THIS ARTICLE AS DOI: 10.1116/6.0002201

- 1 ³⁴ G. P. Kochanski, W. Zhu, Y. Goren, in *Vacuum Microelectronics*, edited by W. Zhu
- 2 (Wiley, New York, 2001), Chap 2.

This is the author's peer reviewed, accepted manuscript. However, the online version of record will be different from this version once it has been copyedited and typeset.
PLEASE CITE THIS ARTICLE AS DOI: 10.1116/6.0002201

1 FIGURE CAPTIONS

2 FIG. 1. Spindt emitter fabrication process: (a) Template cavity formation made of Mo and
3 SiO₂, (b) Al sacrificial layer deposition, (c) Emitter deposition from the substrate normal,
4 (d) lift off by dissolving the sacrificial layer.

5
6 FIG. 2. Cross-sectional SEM image of a Al/Mo/SiO₂ cavity after the Mo emitter deposition.
7 The size of the hole in the cavity was controlled by changing the thickness of Al sacrificial
8 layer.

9
10 FIG. 3. Deposition rate of Mo films measured using QCM monitor at the center of the stage.

11
12 FIG. 4. Cross-sectional SEM images of Mo emitters fabricated inside the Al/Mo/SiO₂ cavity
13 at various anode cap voltages: (a) $V_C = 20$ V, (b) $V_C = 40$ V, and (c) $V_C = 60$ V. The Ar
14 gas pressure was 0.3 Pa. The scale bar of 0.5 μm length is shown at the right-bottom of
15 each figure.

16
17 FIG. 5. Aspect ratio dependence of Mo emitters (a) on the cap voltage and (b) on the Ar gas
18 pressure. The cavity consisted of a hole of diameter 540 nm and SiO₂ layer of thickness
19 280 nm.

20
21 FIG. 6. (a) XRD patterns of Mo films deposited on bare Si substrates at an Ar gas pressure
22 of 0.3 Pa at various cap voltages for 30 min. The baseline of each XRD pattern is shifted
23 by 1×10^6 . (b) Magnified pattern near the Mo (110) peak. Note that the vertical axis is in
24 logarithmic scale. The baseline is not shifted in this figure. The vertical dotted line at $2\theta =$
25 40.55° denotes the Mo (110) that appeared in the powder diffraction data.

26

1 FIG. 7. Stress in Mo films deposited on Si (100) substrates. Negative value denotes
2 compressive stress: (a) cap voltage dependence at Ar gas pressure of 0.3 Pa, (b) Ar gas
3 pressure dependence at $V_C = 40$ V.

4
5 FIG. 8. Cross-sectional SEM images of Mo emitters deposited inside the cavities with
6 different hole sizes: (a) 370 nm, (b) 510 nm, (c) 600 nm, and (d) 795 nm. The SiO₂ layer
7 thickness was 480 nm. The Ar gas pressure and V_C during the emitter growth were 0.3 Pa
8 and 40 V, respectively. The solid yellow line was drawn from the edge of the hole with a
9 9.5-degree tilt (see text).

10
11 FIG. 9. Hole diameter dependence of the aspect ratio of the Mo emitter prepared under Ar
12 gas pressure of 0.3 Pa and at $V_C = 40$ V.

13
14 FIG. 10. Dependence of aspect ratio of Mo emitters on the Ar gas pressure and V_C . The
15 cavity depth was 300 nm, and the hole diameter was 850 nm.

16
17 FIG. 11. Mo emitter of maximum AR value (1.32) obtained under the Ar gas pressure 0.3
18 Pa and at $V_C = 10$ V. The cavity depth was 300 nm, and the hole diameter was 850 nm.

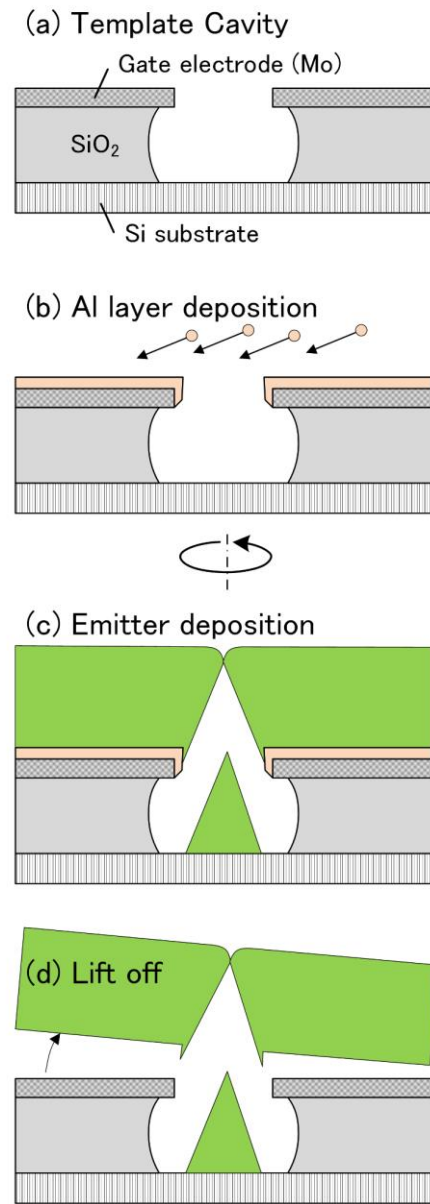


FIG. 1. Spindt emitter fabrication process: (a) Template cavity formation made of Mo and SiO₂, (b) Al sacrificial layer deposition, (c) Emitter deposition from the substrate normal, (d) lift off by dissolving the sacrificial layer.

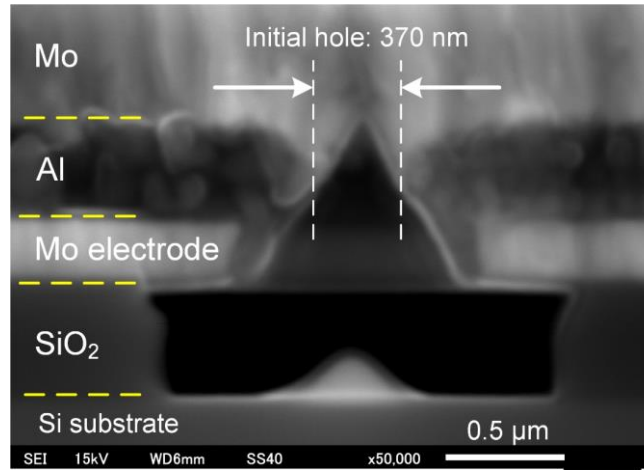


FIG. 2. Cross-sectional SEM image of a Al/Mo/SiO₂ cavity after the Mo emitter deposition. The size of the hole in the cavity was controlled by changing the thickness of Al sacrificial layer.

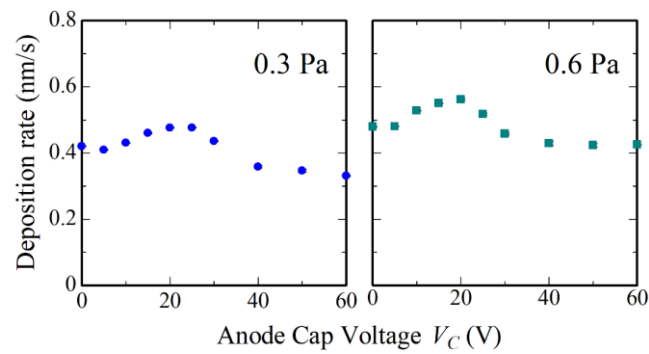


FIG. 3. Deposition rate of Mo films measured using QCM monitor at the center of the stage.

This is the author's peer reviewed, accepted manuscript. However, the online version of record will be different from this version once it has been copyedited and typeset.
PLEASE CITE THIS ARTICLE AS DOI: 10.1116/1.5002201

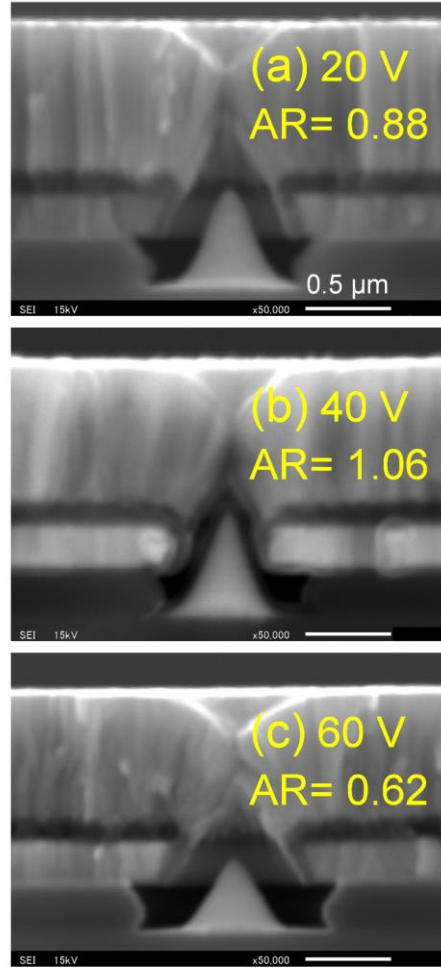


FIG. 4. Cross-sectional SEM images of Mo emitters fabricated inside the Al/Mo/SiO₂ cavity at various anode cap voltages: (a) $V_c = 20$ V, (b) $V_c = 40$ V, and (c) $V_c = 60$ V. The Ar gas pressure was 0.3 Pa. The scale bar of $0.5 \mu\text{m}$ length is shown at the right-bottom of each figure.

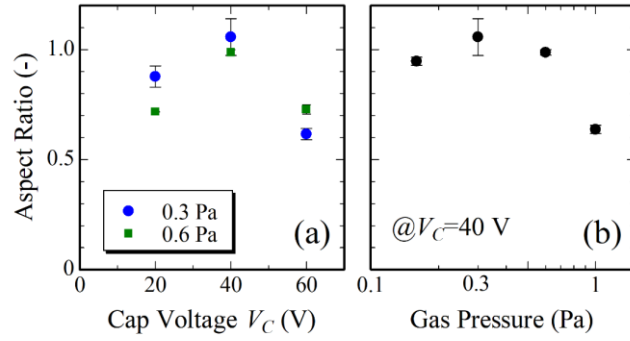


FIG. 5. Aspect ratio dependence of Mo emitters (a) on the cap voltage and (b) on the Ar gas pressure. The cavity consisted of a hole of diameter 540 nm and SiO_2 layer of thickness 280 nm.

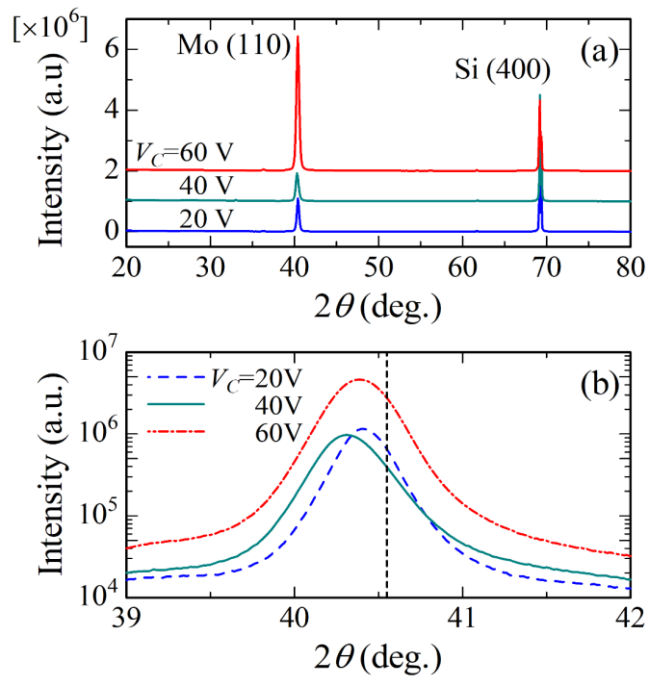


FIG. 6. (a) XRD patterns of Mo films deposited on bare Si substrates at an Ar gas pressure of 0.3 Pa at various cap voltages for 30 min. The baseline of each XRD pattern is shifted by 1×10^6 . (b) Magnified pattern near the Mo (110) peak. Note that the vertical axis is in logarithmic scale. The baseline is not shifted in this figure. The vertical dotted line at $2\theta = 40.55^\circ$ denotes the Mo (110) that appeared in the powder diffraction data.

This is the author's peer reviewed, accepted manuscript. However, the online version of record will be different from this version once it has been copyedited and typeset.
PLEASE CITE THIS ARTICLE AS DOI: 10.1116/6.0002201

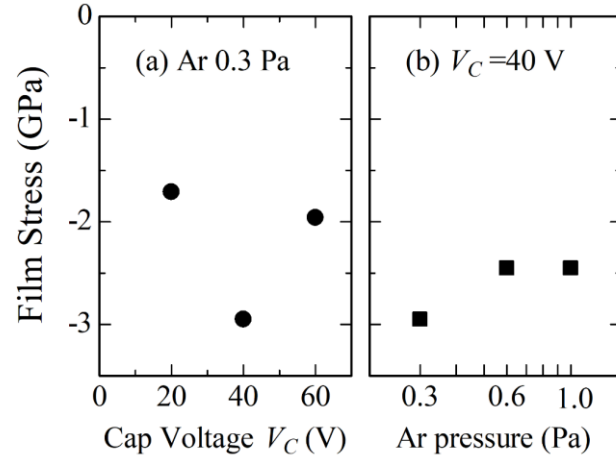


FIG. 7. Stress in Mo films deposited on Si (100) substrates. Negative value denotes compressive stress: (a) cap voltage dependence at Ar gas pressure of 0.3 Pa, (b) Ar gas pressure dependence at $V_C = 40$ V.

This is the author's peer reviewed, accepted manuscript. However, the online version of record will be different from this version once it has been copyedited and typeset.
PLEASE CITE THIS ARTICLE AS DOI: 10.1116/1.5002201

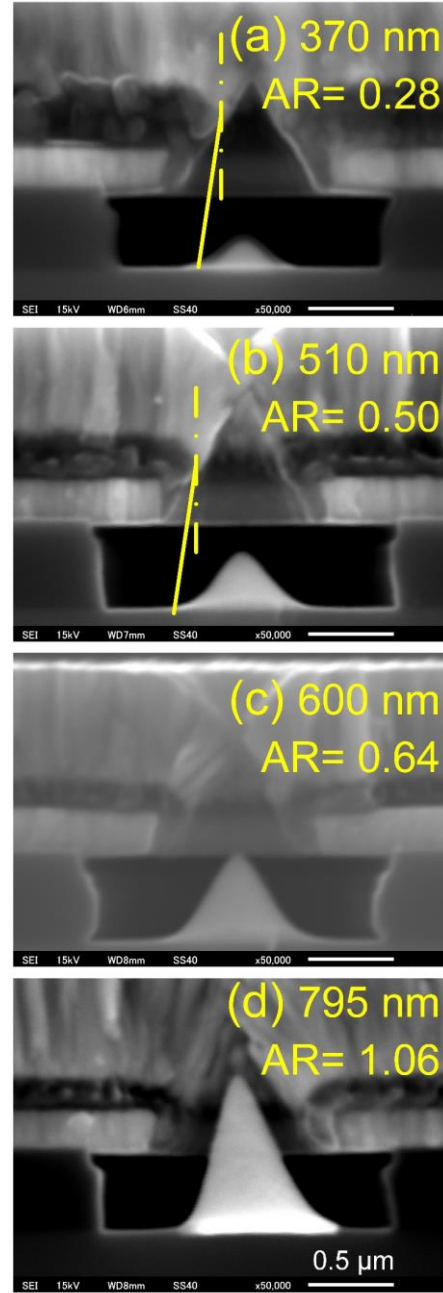


FIG. 8. Cross-sectional SEM images of Mo emitters deposited inside the cavities with different hole sizes: (a) 370 nm, (b) 510 nm, (c) 600 nm, and (d) 795 nm. The SiO_2 layer thickness was 480 nm. The Ar gas pressure and V_C during the emitter growth were 0.3 Pa and 40 V, respectively. The solid yellow line was drawn from the edge of the hole with a 9.5 degree tilt (see text).

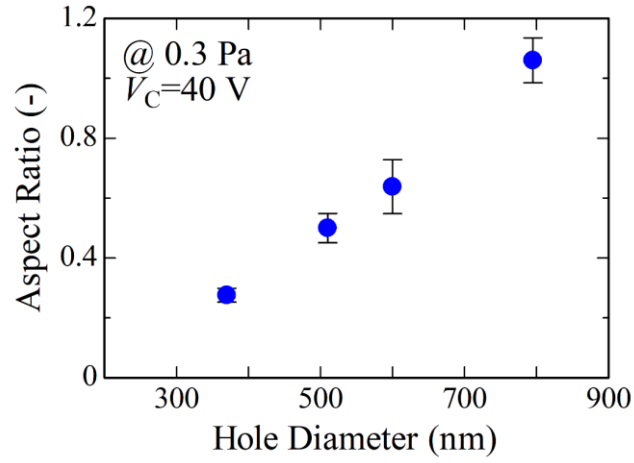


FIG. 9. Hole diameter dependence of the aspect ratio of the Mo emitter prepared under Ar gas pressure of 0.3 Pa and at $V_C = 40$ V.

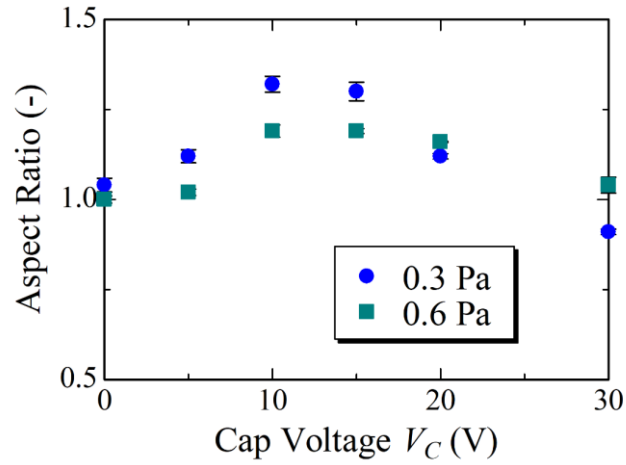


FIG. 10. Dependence of aspect ratio of Mo emitters on the Ar gas pressure and V_C . The cavity depth was 300 nm, and the hole diameter was 850 nm.

This is the author's peer reviewed, accepted manuscript. However, the online version of record will be different from this version once it has been copyedited and typeset.

PLEASE CITE THIS ARTICLE AS DOI: 10.1116/6.0002201

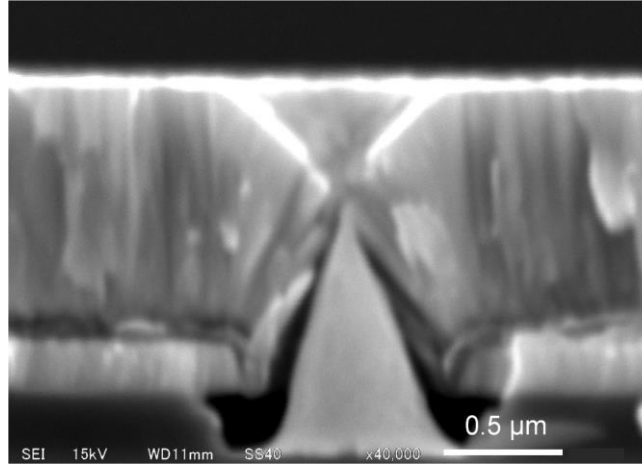
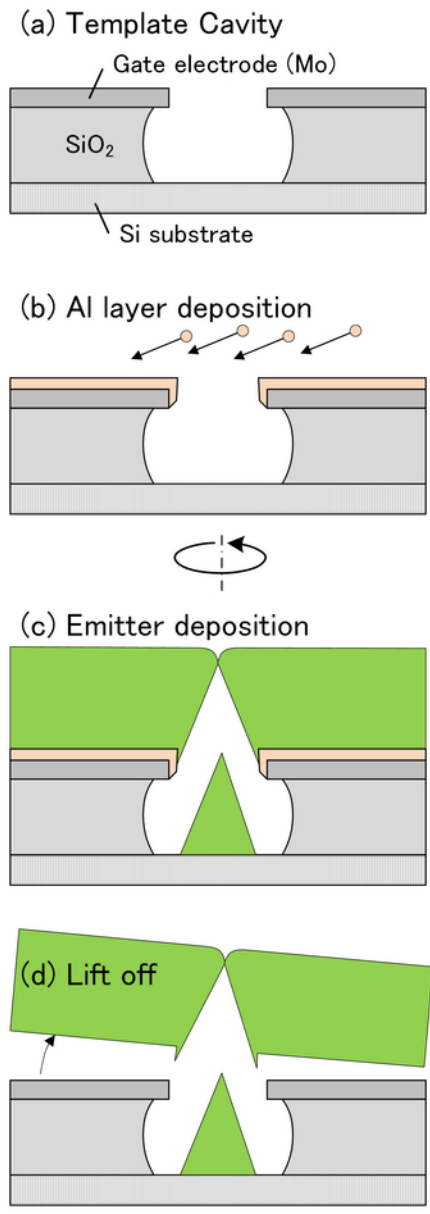
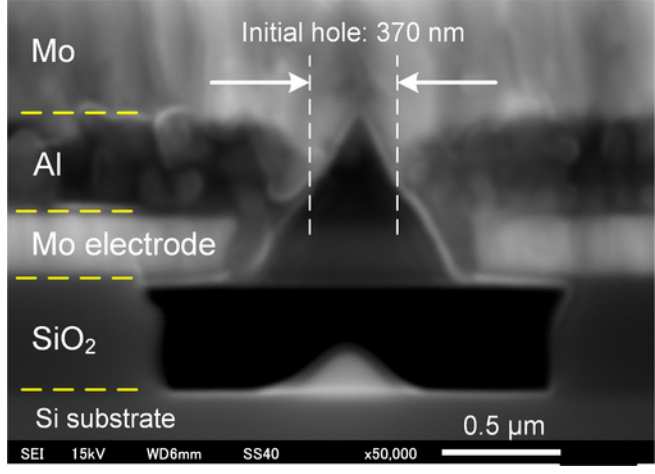


FIG. 11. Mo emitter of maximum AR value (1.32) obtained under the Ar gas pressure 0.3 Pa and at $V_c = 10$ V. The cavity depth was 300 nm, and the hole diameter was 850 nm.

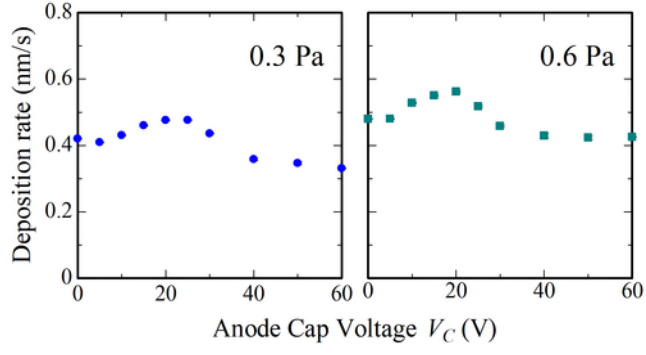
This is the author's peer reviewed, accepted manuscript. However, the online version of record will be different from this version once it has been copyedited and typeset.
PLEASE CITE THIS ARTICLE AS DOI: 10.1116/6.0002201



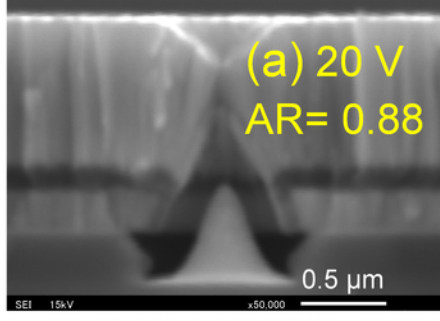
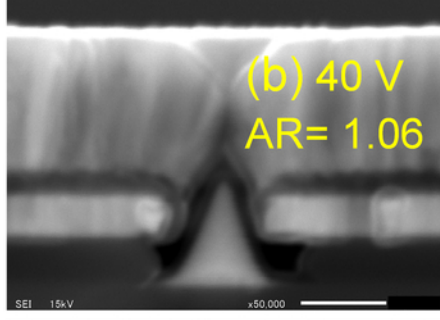
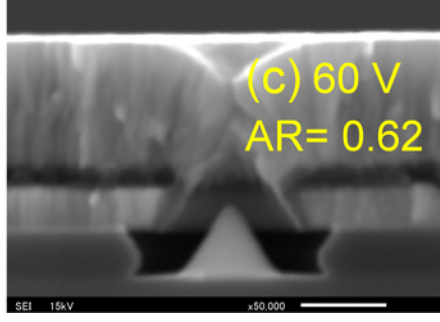
This is the author's peer reviewed, accepted manuscript. However, the online version of record will be different from this version once it has been copyedited and typeset.
PLEASE CITE THIS ARTICLE AS DOI: 10.1116/6.0002201



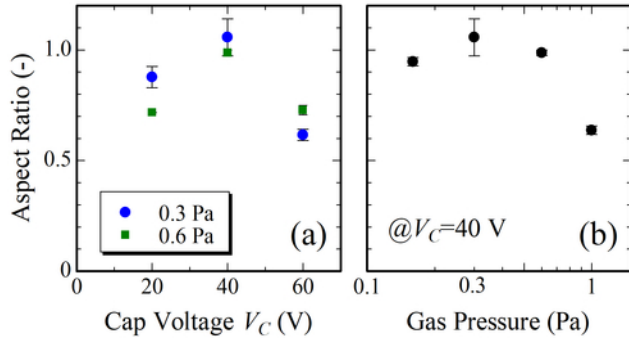
This is the author's peer reviewed, accepted manuscript. However, the online version of record will be different from this version once it has been copyedited and typeset.
PLEASE CITE THIS ARTICLE AS DOI: 10.1116/6.0002201



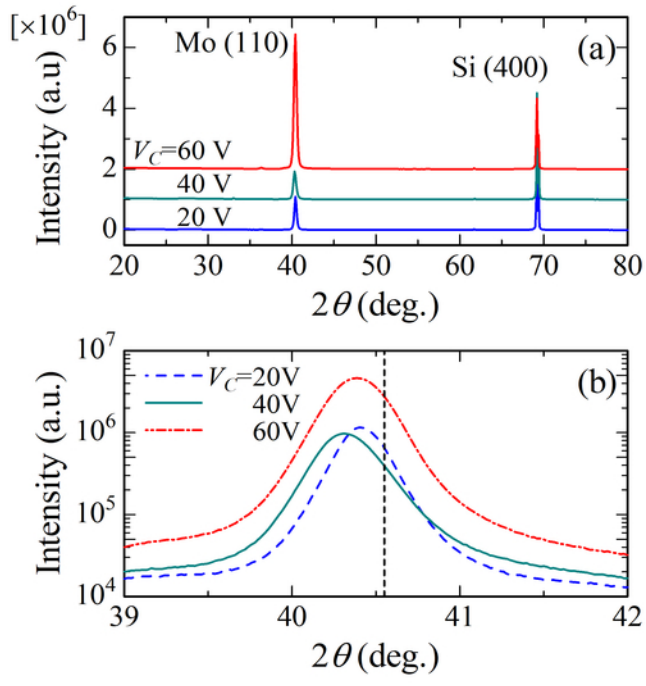
This is the author's peer reviewed, accepted manuscript. However, the online version of record will be different from this version once it has been copyedited and typeset.
PLEASE CITE THIS ARTICLE AS DOI: 10.1116/6.0002201



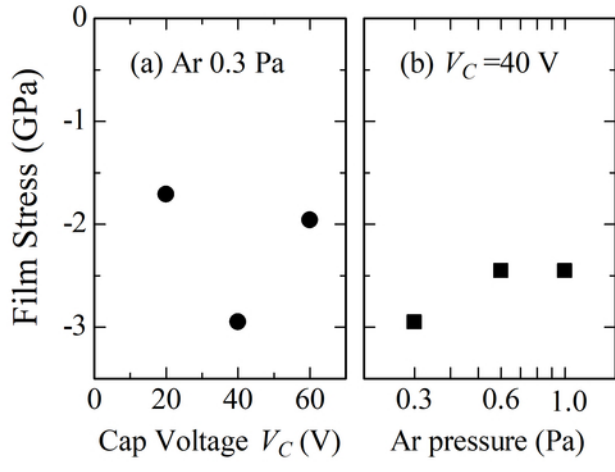
This is the author's peer reviewed, accepted manuscript. However, the online version of record will be different from this version once it has been copyedited and typeset.
PLEASE CITE THIS ARTICLE AS DOI: 10.1116/6.0002201



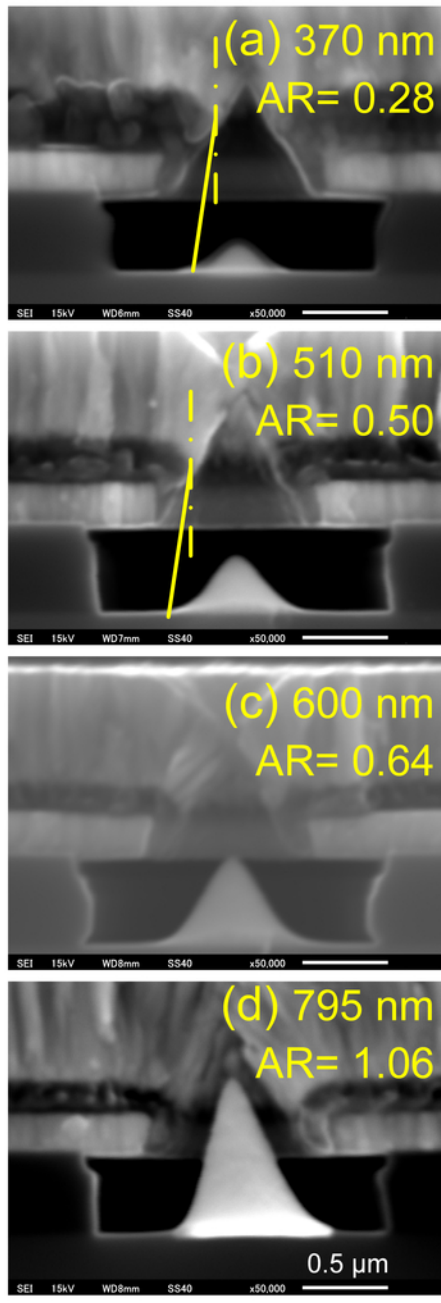
This is the author's peer reviewed, accepted manuscript. However, the online version of record will be different from this version once it has been copyedited and typeset.
PLEASE CITE THIS ARTICLE AS DOI: 10.1116/6.0002201



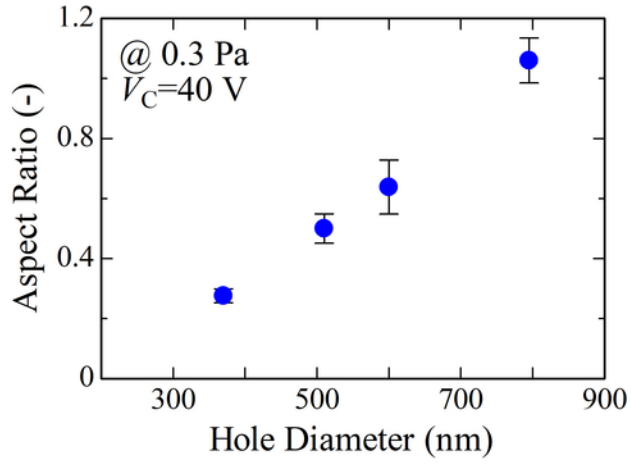
This is the author's peer reviewed, accepted manuscript. However, the online version of record will be different from this version once it has been copyedited and typeset.
PLEASE CITE THIS ARTICLE AS DOI: 10.1116/6.0002201



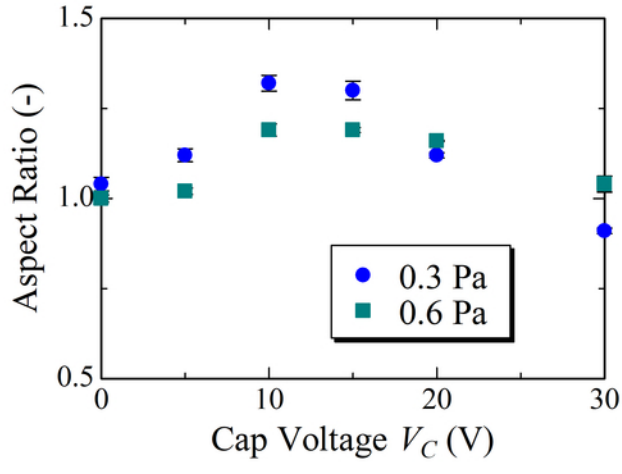
This is the author's peer reviewed, accepted manuscript. However, the online version of record will be different from this version once it has been copyedited and typeset.
PLEASE CITE THIS ARTICLE AS DOI: 10.1116/6.0002201



This is the author's peer reviewed, accepted manuscript. However, the online version of record will be different from this version once it has been copyedited and typeset.
PLEASE CITE THIS ARTICLE AS DOI: 10.1116/6.0002201



This is the author's peer reviewed, accepted manuscript. However, the online version of record will be different from this version once it has been copyedited and typeset.
PLEASE CITE THIS ARTICLE AS DOI: 10.1116/6.0002201





This is the author's peer reviewed, accepted manuscript. However, the online version of record will be different from this version once it has been copyedited and typeset.
PLEASE CITE THIS ARTICLE AS DOI: 10.1116/6.0002201

